

LiDAR-BEVMTN: Real-Time LiDAR Bird’s-Eye View Multi-Task Perception Network for Autonomous Driving

Sambit Mohapatra^{1,3†}, Senthil Yogamani^{2†}, Varun Ravi Kumar¹,
 Stefan Milz⁴, Heinrich Gotzig¹ and Patrick Mäder³ [†]co-first authors
¹Valeo, Germany ²Valeo, Ireland ⁴SpeenLab.ai, Germany ³TU Ilmenau, Germany

Abstract—LiDAR is crucial for robust 3D scene perception in autonomous driving. LiDAR perception has the largest body of literature after camera perception. However, multi-task learning across tasks like detection, segmentation, and motion estimation using LiDAR remains relatively unexplored, especially on automotive-grade embedded platforms. We present a real-time multi-task convolutional neural network for LiDAR-based object detection, semantics, and motion segmentation. The unified architecture comprises a shared encoder and task-specific decoders, enabling joint representation learning. We propose a novel Semantic Weighting and Guidance (SWAG) module to transfer semantic features for improved object detection selectively. Our heterogeneous training scheme combines diverse datasets and exploits complementary cues between tasks. The work provides the first embedded implementation unifying these key perception tasks from LiDAR point clouds achieving 3ms latency on the embedded NVIDIA Xavier platform. We achieve state-of-the-art results for two tasks, semantic and motion segmentation, and close to state-of-the-art performance for 3D object detection. By maximizing hardware efficiency and leveraging multi-task synergies, our method delivers an accurate and efficient solution tailored for real-world automated driving deployment. Qualitative results can be seen at <https://youtu.be/H-hWRzv2IIY>.

I. INTRODUCTION

LiDAR sensors have become common in autonomous driving assistance sensor suites [1]. It is more expensive than cameras and radars, but they provide superior 3D point clouds needed for accurate 3D scene understanding [2], [3]. It is also more robust to challenging conditions like low light and adverse weather [4], [5], [6]. Processing sparse 3D LiDAR point clouds is computationally intensive, and alternate 2D simplified representations such as range images and Birds Eye View (BEV) representations are commonly used for improving efficiency. There are only a few papers that explore this in the literature, and none of these focus on automotive-embedded platform implementations.

In deep learning, our primary focus is often on optimizing a specific metric, such as achieving a high score on a benchmark or improving key performance indicators for a business. This optimization process typically involves training a single model or a group of models to perform the desired task. Through fine-tuning and iterative adjustments, we strive to reach a point where the model’s output no longer shows significant improvements. While this approach often yields satisfactory results, it overlooks specific details that could enhance performance on the targeted metric. This narrow focus on a single task disregards the knowledge that could be gained from related tasks during the training process. We can improve the model’s generalization capabilities for the original task by explicitly

leveraging the training signals from these related tasks. This methodology is called Multi-Task Learning (MTL), unlike single-task learning.

In the context of MTL, we can extract valuable insights and conclusions when multiple loss functions are being optimized. Even in cases where only one loss is being optimized, there is typically an auxiliary task that can enhance the performance of the primary task. Employing an efficient multi-task model offers numerous advantages over multiple single-task models, including improved performance in embedded systems, certification, validation, and testing. Moreover, deploying a single MTL model is more straightforward than managing several independent single-task learning (STL) models.

In the context of autonomous driving with LiDAR, MTL holds great importance, as it enables the exploitation of shared knowledge from various related tasks, ultimately leading to improved perception and decision-making in autonomous vehicles. When jointly trained, different tasks have a regularizing effect on each other, reducing overfitting issues. While achieving different end goals, features learned by tasks generally have a fair amount of overlap. This makes it possible to use features from one task as additional input to another. This is also something we have leveraged in this work.

This work presents a multi-task CNN for real-world use cases and deployment scenarios. Concretely, we design a CNN that performs object detection, semantic segmentation, and motion segmentation with LiDAR point clouds. The fundamental motivation behind a multi-task network is to reduce the memory and computation requirements while executing several parallel tasks on resource-constrained embedded computers, and we demonstrate this with our experiments with embedded automotive hardware platforms.

Our main contributions to this work include the following:

- We demonstrate a real-time multi-scan multi-task CNN architecture for joint object detection, semantic segmentation, and motion segmentation from LiDAR point clouds.
- We propose a Semantic Weighting and Guidance (SWAG) module that selectively transfers relevant semantic features to improve object detection accuracy.
- A heterogeneous training strategy combining diverse datasets and leveraging multi-task synergies.
- We propose a simple yet effective range-based point cloud densification technique to enrich object boundaries and improve long-range detection.
- We perform extensive ablation studies and demonstrate the real-time capabilities on an embedded platform - the NVIDIA Xavier AGX development kit.

II. RELATED WORK

In this section, we review relevant literature on the three key LiDAR-based perception tasks addressed in our work - object detection, semantic segmentation, and motion segmentation. We first discuss recent approaches that tackle each task independently. We then examine prior multi-task methods that aim to solve subsets of the tasks jointly.

Our goal is to provide background on the single-task state-of-the-art, highlight limitations of independent modeling, and motivate the need for multi-task learning across all three modalities. This sets the stage for our proposed LiDAR-BEVMTN framework which unifies these complementary perception tasks in a joint representation learning paradigm.

A. Object detection

Object detection is finding objects of interest in a scene and localizing them with an oriented bounding box. It is typically done on a per-frame basis. However, using multiple motion-compensated past frames can improve detection accuracy significantly, particularly for slow-moving and static objects, as it allows more observations. Object detection is a crucial component of almost any Autonomous Driving (AD) stack since this is crucial for functions like collision avoidance, object tracking, and emergency braking. It also supports other AD tasks in achieving various end-user functions.

Architectures for object detection are broadly divided into 2-stage region proposal and refinement methods and single-stage methods. Due to the inherent architecture, 2-stage methods tend to be slower while generally more accurate. Some early work like [7], [8] first group 3D point cloud into 3D tensors called voxels and then use 3D convolutions on the voxels. However, 3D convolutions have proved to be too slow for real-time operation. This approach was improved by [9], which uses sparse convolutions applied on voxel-wise features for fast inference. They also introduce a widely used data augmentation technique where object point clouds are sampled from the training set and introduced into different point clouds to solve the problem of relatively few objects in the dataset [10]. However, at 50ms per frame inference time, they are still unsuitable for real-time operation. Another 2-stage method that improved the Average Precision (AP) for object detection was [11], which tries to remove the large number of anchor boxes used in traditional object detection by first learning point-wise features using [12] for segmenting the point cloud into foreground and background points and simultaneously generating a small number of proposals. The second stage then refines these proposals for 3D box regression. While introducing some novel concepts, the network relies on effective segmentation of foreground and background points which can become difficult at long range due to extreme sparsity and occlusion. This is also seen in the results' relatively significant AP drop for hard category objects. More recently, [13] proposed another 2-stage voxel-point hybrid method that achieves state-of-the-art performance in terms of Average Precision (AP) on the KITTI and Waymo datasets [14]. They learn features on a point and voxel level using a 3D CNN to learn voxel-wise features and then reduce the feature space by a small set of

keypoint features. More recently, [15], [16] proposed a multi-modal approach to fuse features from images and LiDAR point clouds that achieves high KITTI benchmark scores. However, our work is focused on LiDAR-only approaches.

Among single-stage approaches, methods like [17], [18] project 3D point cloud to 2D BEV representation and apply efficient 2D convolutions for fast object detection. A similar approach is followed by [19], which uses an Euler region proposal network for complex-valued orientation regression. Our previous work *BEVDetNet* [17] achieves an impressive inference latency of 6ms per frame on Nvidia Xavier AGX. Nevertheless, a significant challenge such grid-based methods face is that the sparsity of the 3D point clouds leads to many empty cells in the grid, which negatively impacts performance. Another seminal work is [20], which uses a particular pillar-encoding layer to generate a pseudo-2D representation of point cloud and then uses Single Shot Detector (SSD) [21] style heads for bounding box prediction. However, this additional pre-processing layer and many anchor boxes used in SSD-style detection heads are detrimental to the real inference frame rate. Similarly, [22] also employ an SSD-based teacher-student architecture where two identical SSD networks are used as a teacher and student. The teacher is trained directly using the ground truth annotations. The student uses the teacher's predictions and the ground truth annotations to train using a consistency loss and an orientation-aware distance-IoU loss, respectively. However, the dependency on the teacher's prediction also makes the student vulnerable to bad-quality soft targets from the teacher network. Also, this dual network architecture doubles the amount of GPU memory and compute power needed and hence would only be suitable for real-time applications on embedded targets. This is evident in its relatively large inference time of 30ms per frame.

B. Semantic Segmentation

Semantic segmentation refers to assigning a semantic label to each pixel or point in the scene. This way, each observation is labeled into one of the predetermined semantic classes. Again, this can be done on single frames or using several past frames. This is useful for automotive applications such as free space estimation, drivable area estimation, path planning, lane marking, and general refinement of object detection [23], [24]. As with object detection, we mainly focus on LiDAR-only methods and include published work using the SemanticKITTI [25] dataset. [26], [27] transformed 3D point cloud into 2D representation using spherical projection and then used a [28] based CNN followed by refinement using conditional random field [29] module for semantic segmentation. This was improved upon by! [30], which uses a similar spherical projection called range images and a [31] based architecture to perform fast semantic segmentation. However, range images (spherical projection used in all these approaches) do not allow easy fusion of features with that of the grid-based 2D representations typically used for object detection networks in a multi-task approach. Another novel approach was proposed by [32] where a teacher-student architecture is employed. The much larger teacher model is used to collect point and voxel-wise features from the input point cloud, and this information

is then distilled into the smaller student model. Concretely, they divide the point cloud into a set of voxels and then take a subset based on distance and difficulty criteria. They then compute a similarity loss between the point and voxel features. However, the use of 3D convolutions is not suitable for real-time operation and does not fit the case of multi-task learning with 2D grid-based inputs. Furthermore, the teacher-student architecture makes joint training difficult, as in our case.

C. Motion Segmentation

Motion segmentation is a particular case of semantic segmentation where there are only two classes - motion and static, denoting pixels or points that are dynamic or static, respectively. However, in contrast to semantic segmentation, motion segmentation needs at least two successive frames since motion cannot be inferred from a single observation. Typically, many consecutive frames are used to achieve higher accuracy in motion segmentation. Motion segmentation finds key uses in systems like Simultaneous Localization and Mapping (SLAM), object tracking, collision avoidance, and path planning systems of the AD stack. While we have discussed several approaches for semantic segmentation, there needs to be more work for moving object segmentation - a more specialized case of semantic segmentation. One of the most notable is [33], which uses multiple frames of point clouds converted into a spherical coordinate system (range image) to segment moving pixels. The authors' motion compensates the frame and computes successive frames' differences, which helps provide motion cues. A standard encoder-decoder architecture is then used to predict a motion mask for the most recent frame. While simple and effective, their best results are achieved with eight past frames, again prohibitive from the memory and computing perspective of embedded targets in real-world applications. Also, the range view skews the aspect ratio, making fusing learned features across tasks in a multi-task scenario very hard. We use a similar idea in our previous work [34], using only two past frames in a BEV space to segment motion pixels. More recently, [35] proposed a dual encoder approach to extract spatial and temporal features and fuse them using a sparse 3D convolution module. They show improved accuracy, but the dual encoder architecture directly opposes a multi-task approach, where having a single encoder is one of the critical requirements. Also, the use of 3D convolutions is not suitable for low latency, and this shows in their rather large run times.

D. Multi-task LiDAR perception

Compared to other modalities such as image-based [36], [37] and fusion-based approaches [38] for multi-task perception networks, there are rather few methods for LiDAR, only multi-task perception. Our choice of LiDAR-only multi-task perception is based on the fact that LiDAR as a sensor sits in a sweet spot between sensors such as cameras which produce dense data but are severely affected by environmental conditions such as ambient light, rain, fog, etc., and radars which have the longest range produce data that is too sparse

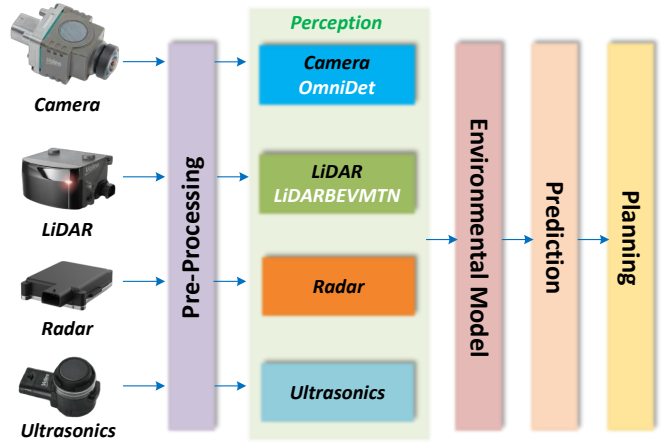


Fig. 1: High-level Architecture of Level 2/Level 3 Autonomous Driving System.

for tasks like object detection and semantic segmentation. Furthermore, we tailor our application with real-time deployment with embedded hardware in mind and choose a 2D BEV representation. This enables us to use fast 2D convolutions in the architecture and also makes the output readily usable with other AD functions, such as path planning, with very little post-processing needs. Among multi-task LiDAR-only approaches, [39] uses a single point cloud and performs object detection, semantic segmentation, and panoptic segmentation. They employ 3D sparse convolutions as feature extractors and then project features to a 2D BEV space for contextual feature aggregation. This is then fed to task heads in BEV space for final outputs. Another interesting approach is [40], which does object detection and scene flow using two consecutive frames of LiDAR point clouds. However, they follow a two-encoder architecture for feature extraction from each stream and then fuse them using a joint encoder stage. This is inefficient from a computation latency perspective. Similarly, [41] uses an encoder-decoder architecture with sparse 3D convolutions for object detection and segmentation of roads into different parts.

III. PROPOSED METHOD

A. System Architecture

Fig. 1 shows a typical level 2 and 3 AD system architecture layout. A multi-modal sensor suite is used for environmental sensing. We have demonstrated the most common combination comprising the camera for surround view at short and mid-range, LiDAR at mid to long-range 3D sensing, radar for medium to ultra-long-range sensing, and ultrasonic sensor for short-range sensing low-speed maneuvers such as automatic parking. This work uses data sets collected using top-mounted rotating LiDAR sensors. Data from the sensors pass through the pre-processing stage into the perception stage, where individual modalities pass through their perception algorithms and, optionally, fusion-based algorithms. Our work corresponds to the LiDAR perception section (shown in the figure). It builds on our previous work *OmniDet* [42] is a multi-task camera perception model. Outputs from the perception stage then feed into the environmental model, which constructs a

detailed model of the ego vehicle state and other actors in the environment and localizes the ego vehicle in the environment model. Tracking algorithms in the prediction stage then predict the successive states of all actors, and finally, the planning stage provides motion planning for the next time step. Having established the overall picture, the following sections explain our work in greater detail.

B. Input Pre-processing

The Bird’s Eye View (BEV) representation transforms 3D point clouds into a 2D grid structure while preserving key information. Each point $\mathbf{p} = (x, y, z)$ is mapped to a cell (u, v) in the BEV image $I_{BEV} \in \mathbb{R}^{H \times W}$ based on its x-y location:

$$u = \left\lfloor \frac{x - x_{min}}{r_x} \right\rfloor, v = \left\lfloor \frac{y - y_{min}}{r_y} \right\rfloor \quad (1)$$

where (x_{min}, y_{min}) are the lower bounds of the BEV range, and (r_x, r_y) define the cell resolution. Point features like depth, intensity, etc., are aggregated in the corresponding cell. This enables efficient 2D convolutions without losing substantial information.

Crucially, BEV preserves aspect ratios as objects maintain consistent dimensions with distance. The compact BEV representation also simplifies integration with downstream modules for planning and prediction. As in [17], we use a $60m \times 60m$ BEV range with **0.125m** resolution, filtering points outside the view. The resulting $I_{BEV} \in \mathbb{R}^{480 \times 480 \times C}$ retains high-fidelity scene representations for multi-task learning.

Range-based point cloud densification: We propose a simple yet effective range-based point cloud densification technique that can improve point density along the depth dimension even at test time. We convert every 3D point $\mathbf{p} = (x, y, z)$ to its spherical coordinates - range (r), azimuth (ϕ), and elevation (θ):

$$r = \sqrt{x^2 + y^2 + z^2} \quad (2)$$

$$\theta = \sin^{-1} \left(\frac{z}{r} \right) \quad \text{elevation angle} \quad (3)$$

$$\phi = \tan^{-1} \left(\frac{y}{x} \right) \quad \text{azimuth angle} \quad (4)$$

We then increase range by $\Delta r \in [0.1, 0.3]$ and recompute the new densified points’ Cartesian coordinates (x', y', z') as:

$$x' = (r + \Delta r) \cos \theta \sin \phi \quad (5)$$

$$y' = (r + \Delta r) \cos \theta \cos \phi \quad (6)$$

$$z' = (r + \Delta r) \sin \theta \quad (7)$$

Since only the range is modified, the new points trace along the depth of objects, improving density in the depth dimension. This is particularly beneficial when projected to BEV, enhancing visibility along the depth axis. However, over-augmentation can cause points to leave object boundaries. We conduct ablation experiments for object detection, as this augmentation modifies ground truth for segmentation. Fig. 2 illustrates the point densification effects. The proposed technique provides a simple but effective way to enrich point density at test time.

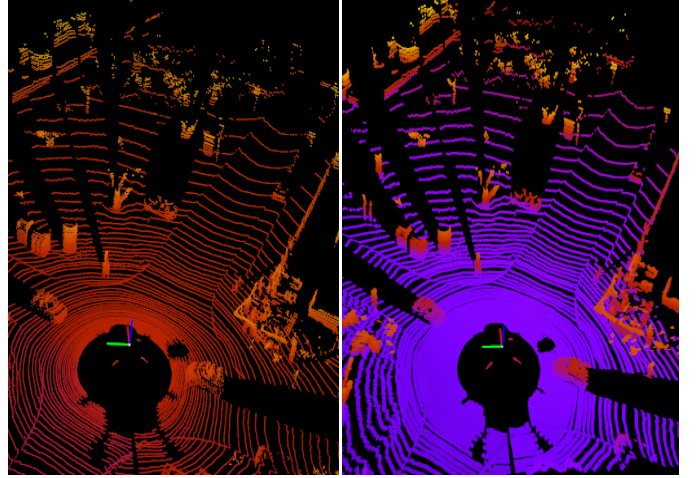


Fig. 2: **Illustration of proposed Range based point cloud densification** - Raw point cloud (left) and densified point cloud (right).

C. Network Architecture

Our network adopts an encoder-decoder convolutional neural network (CNN) backbone for feature extraction, followed by task-specific decoders and output heads (Fig. 3). The encoder comprises a shared multi-scale feature extractor based on a ConvNeXt-style architecture. It outputs a pyramidal hierarchy of features that encode increasing semantic complexity while reducing spatial dimensions.

The core design principle is to leverage complementary cues from the different tasks during the encoder and decoder stages. The encoder features are directly fed to a decoder and pixel-wise classification head for semantic segmentation.

For object detection, we introduce a Semantic Weighting and Guidance (SWAG) unit that selectively incorporates semantic features to improve detection performance. Specifically, the encoder features are fed to the semantic and detection decoders. The SWAG module computes a relevance match between intermediate features from both branches. This match vector is used to weight the semantic features before fusing them with the detection features. By learning to select useful semantic cues, SWAG provides improved generalization. Our box regression scheme based on key points representing object centers and orientation and dimension prediction heads allows high-density prediction while preventing collisions.

As in our previous work [17], we represent objects as key points, where a key point $\mathbf{p}_i \in \mathbb{R}^2$ marks the i^{th} object’s center location in the BEV image. This allows high-density prediction while preventing collisions, as the object’s body ensures overlap does not occur.

Corresponding to each key point \mathbf{p}_i , we also predict the object’s orientation θ_i as a binned classification between $[0, 180]$ degrees with a bin size of $\Delta\theta = 5$ degrees:

$$\theta_i = \arg \max_j \{z_{ij}\} \quad \text{where } j \in \{0, \frac{180}{\Delta\theta} - 1\} \quad (8)$$

where $\mathbf{z}_i \in \mathbb{R}^{180/\Delta\theta}$ is the predicted classification logit vector for object i . Additionally, a box dimension prediction head is added to regress the width w_i and length l_i for each detected object i :

$$w_i = f_w(\mathbf{v}_i) \quad l_i = f_l(\mathbf{v}_i) \quad (9)$$

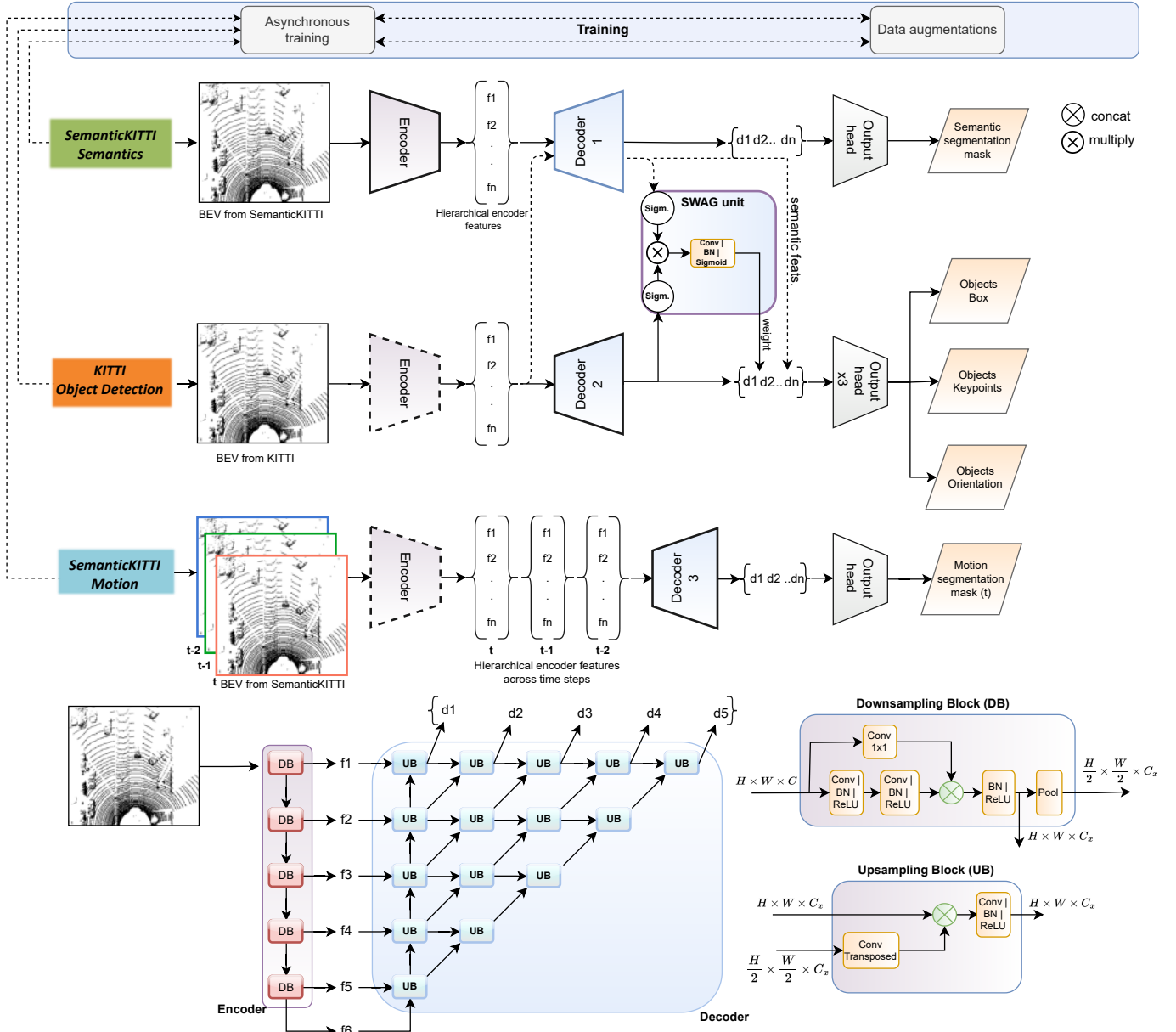


Fig. 3: **LiDAR-BEVMTN multi-task learning architecture.** Top: High-level view showing shared encoder and task-specific decoders. Bottom: Encoder and decoder sub-modules details. Key features: 1) Shared encoder for unified feature extraction 2) SWAG module for cross-task interactions 3) Asynchronous training across datasets 4) Task-specific decoders enable multi-task pixel-level prediction.

where \mathbf{v}_i contains box regression features and f_w, f_l denotes width and length prediction layers. As the semantic segmentation head trains, its accuracy improves over time. This enhances the quality of semantic features contributed to the object detection head via the proposed SWAG unit, leading to increased detection performance.

Motion segmentation operates on multi-frame input, with the encoder applied individually to each frame. The resulting features are concatenated temporally and compressed before feeding to the motion decoder and segmentation head. Unlike semantics, motion patterns can be negatively impacted by semantic errors; hence semantic guidance is excluded.

The proposed architecture unifies multiple perceptual tasks through shared encoding, selectively leverages cross-task interactions, and employs task-specific decoding to balance

joint representation learning with specialized prediction. This achieves significant performance gains in each task compared to independent modeling.

Encoder and Decoder: The encoder comprises 5 cascaded downsampling blocks (DB) as seen in Figure 3 (bottom right) based on a modified ConvNeXt-style [43] architecture. Each DB contains convolutional layers followed by batch normalization and ReLU activation, configured in a residual block structure. Compared to a standard ConvNeXt block, the key modification is that two outputs are generated from each DB - one retaining the original spatial resolution and another with 2x downsampling applied.

Specifically, each DB first applies a strided 3x3 convolution with stride 2 to downsample the input feature map. This downsampled output is then fed to the next DB in the cascade.

Meanwhile, the original high-resolution input goes through a residual path consisting of two 3x3 convolutions with batch normalization and ReLU. This produces an output feature map with the same resolution as the input. After the cascaded DB stages, the encoder outputs a set of multi-scale feature maps consisting of the high-resolution outputs from each DB and the low-resolution output of the final DB. This pyramidal hierarchy encodes rich semantic features while preserving spatial details.

The decoder module adopts an expansive pathway that selectively progressively fuses the encoder feature maps. It consists of a series of upsampling and concatenation blocks. Each block upsamples the lower-resolution input using a transposed convolution layer to match the size of the corresponding high-resolution encoder output. The upsampled features are then concatenated channel-wise with the encoder output before going through additional convolutional layers. This learnable feature fusion allows the combining of semantics from the downsampled stream with spatial details from the high-resolution stream. The progressive fusion through the decoder recovers fine-grained spatial information while leveraging context from the encoder. The final output is a dense feature map with the same spatial dimensions as the input image, which can be tasked with pixel-level prediction.

Overall, the proposed encoder-decoder architecture provides an effective backbone for multi-task dense prediction, achieving a balance between semantic abstraction and spatial precision.

Semantic Weighting and Guidance (SWAG) unit: The goal of the SWAG unit is to introduce a weighted set of semantic features produced by feeding object detection encoder (the encoder is still the same for all tasks) features into the semantic decoder. A simple but naive approach to introducing semantic features into object detection would be just concatenating them together. However, not all features from the semantic head are equally helpful for the object detection head. Let $f_{sem} \in \mathbb{R}^{H \times W \times C}$ and $f_{od} \in \mathbb{R}^{N \times D}$ denote the intermediate feature maps from the semantic segmentation and object detection decoder branches respectively, where H, W are spatial dimensions, C is number of semantic channels, N is number of candidate boxes, and D is the feature dimensionality for each box. To compute the relevance match, we first apply MLPs to project each into a joint K-dimensional embedding space:

$$h_{sem}(f_{sem}) = \sigma(W_1^{sem} f_{sem} + b_1^{sem}) \quad (10)$$

$$h_{od}(f_{od}) = \sigma(W_1^{od} f_{od} + b_1^{od}) \quad (11)$$

Where: $h_{sem}()$ and $h_{od}()$ are the MLP projections σ is the sigmoid activation function W_1^{sem} and W_1^{od} are the projection weight matrices b_1^{sem} and b_1^{od} are the bias terms f_{sem} and f_{od} are the input feature maps.

Our proposed SWAG module computes a match m between object detection features and semantic output:

$$m = \sigma(h_{od}(f_{od})) \odot \sigma(h_{sem}(f_{sem})) \quad (12)$$

where h_{od} and h_{sem} are small MLPs, σ is the sigmoid function, and \odot is element-wise multiplication between the

embeddings. MLPs are induced to provide learnable nonlinear projections that map detection and segmentation features to a common embedding space where their joint relationships can be effectively modeled and leveraged to improve detection performance. The learnable nature and joint trainability are key advantages over using a fixed projection. This match vector captures the relevance of each semantic feature to object detection. To convert the match to a set of learnable weight vectors w , we apply another conv layer:

$$w = \sigma(CB(m)) \quad (13)$$

where $CB(\cdot)$ denotes a convolution + batch norm layer, and $w \in \mathbb{R}^C$ contains the weighting coefficients. The weighted semantic features $f'_{sem} = w \odot f_{sem}$ are then concatenated with f_{od} for the object detection head, as shown in Fig. 3. The learnable projections and weightings allow SWAG to focus on useful semantic cues automatically. In this way, SWAG learns to select the most relevant semantic features to incorporate into object detection, improving generalization. While SWAG is not explicitly used on the other branches, it generally affects car segmentation across all tasks due to the shared encoder.

D. Training Strategy

A key contribution of our work is a heterogeneous training scheme that unifies diverse datasets across multiple perception tasks. We leverage KITTI [10] for object detection and SemanticKITTI [25] for semantic and motion segmentation. To handle differences in dataset scale and image sequence, we propose a tailored strategy:

- For object detection, each KITTI frame is converted to BEV and used to train the detection branch.
- Semantic segmentation is trained on every 5th SemanticKITTI frame in BEV view. This balances the sample count across tasks.
- For motion segmentation, we identify SemanticKITTI frames with $> \delta$ moving pixels. Each frame and its past two motion-compensated frames are used as inputs, as described in [34].

A key novelty is computing pseudo-residuals to enable joint encoding. For motion frames, residuals between the current and past frames highlight dynamics. For static frames, we self-multiply the depth channel and normalize it to create disparity, improving detection and semantics. The benefit of doing this rather than just repeating the depth channel is that multiplying increases the disparity between high and low height points due to decimal multiplication and helps detection and segmentation.

Standard augmentations like flip, rotation, and dropout are also applied. The proposed heterogeneous training uniquely combines diverse data sources and leverages multi-task interactions to enable unified perception. Our scheme balances sample counts and creates cross-task synergies within a multi-sensor setting.

Asynchronous Training: We propose an asynchronous training strategy since SemanticKITTI and KITTI have unequal training frames for object detection, semantic segmentation, and motion segmentation. For object detection, we

use **5,957** labeled training frames and apply sampling data augmentations to get a total of **9,400** training frames. **9,560** training frames are used for semantic segmentation, and for motion segmentation, we have **4,719** training frames. To handle this imbalance, we adopt an asynchronous training approach. The batch index in our unified data loader runs over the most extended dataset - **9,400** frames for object detection. We remap the index for semantic segmentation by taking a modulo with **9,560**; for motion segmentation, we take a modulo of the batch index with **4,719**. This way, the object detector sees the entire dataset in each training epoch while the semantic and motion networks cycle through their smaller labeled sets multiple times. The three models are trained jointly in an end-to-end manner despite the unequal supervision. We find this asynchronous strategy crucial to train the multi-task model effectively. By aligning the batch indices asynchronously, we can maximize the utilization of the available supervision for each task. Our experiments validate the benefits of this tailored asynchronous training approach for joint perception on KITTI and SemanticKITTI. The index remapping is expressed as:

$$index_{remapped} = index \pmod{L_{dset}} \quad (14)$$

Where:

- $index \in [0, N]$: Batch counter index, ranging from 0 to N
- N : Length of largest dataset
- $index_{remapped}$: Remapped index for current dataset
- L_{dset} : Length of current dataset

We also perform data augmentation, which is crucial for improving the generalization and robustness of deep learning models. However, the effectiveness of augmentation techniques can vary across different tasks. To address this, we adopt a *progressive data augmentation* strategy that gradually increases the complexity of augmentations as the training progresses. In the beginning, when the semantic and motion segmentation networks are primarily training on their smaller labeled sets, we apply more aggressive augmentations specific to those tasks. As the training advances and the object detection network gets exposed to the entire dataset, we introduce fewer task-specific augmentations. This progressive augmentation strategy allows the models to benefit from task-specific augmentation when it matters the most.

IV. EXPERIMENTAL RESULTS

A. Implementation

We employ Pytorch [44] and follow a joint multi-task learning strategy to train the object detection, semantic segmentation, and motion segmentation tasks concurrently. A total of **3** BEV frames is input to the network - one for each task from their respective datasets. Each BEV has the same set of feature channels. The BEV consists of **3** successive frames for motion segmentation and has three times the number of channels. Internally, the network isolates these and computes features for each time step, as discussed in the previous section.

Asynchronous batch sampling accounts for the large disparity between KITTI and SemanticKITTI labeled frames. We

subsample **1524** KITTI validation frames for object detection and use sequence 08 from SemanticKITTI for segmentation. For generalizability, we report semantic segmentation on the most common classes in KITTI. Also, since cars make up the majority of object types in the KITTI dataset, we train for car detection on it. This also affects the other tasks due to the shared architecture. Hence, we report results for the most commonly occurring classes out of the **19** classes generally seen in the semantic segmentation benchmark on SemanticKITTI. The training uses the Adam [45] optimizer with a cosine annealing learning [46] rate over **120** epochs on an Nvidia A100 GPU.

1) *Losses*: We use Focal loss [47] for all classification tasks, L_{cls} - object key point head (L_{kp}), object orientation head (L_{rot}), semantic segmentation head (L_{sem}) and motion segmentation head (L_{mot}) and, smooth-L1 loss [48] is used for all regression, L_{regr} - object box head (L_{box}). The regression loss is only computed for key point locations by masking off other locations in both the ground truth and the predictions. The total loss is then computed as a weighted sum of all losses. We adopt a rotating weighting strategy where the weights are selected from a fixed set of weights proportional to the magnitude of each loss.

$$L_{cls} = -(1 - p)^\gamma \log(p) \quad (15)$$

Where L_{cls} is the classification loss, p is the probability of correct classification, and γ is a hyperparameter.

$$L_{regr} = \begin{cases} 0.5(Y_{hat} - Y)^2/\beta, & |Y_{hat} - Y| < \beta \\ |Y_{hat} - Y| - 0.5\beta, & \text{otherwise} \end{cases} \quad (16)$$

Where L_{regr} is the regression loss, Y_{hat} is the predicted value, Y is the target value, and β is a hyperparameter.

$$L_{total} = \sum_{i=1}^5 w_i L_i \quad (17)$$

Where $L_i \in L_{kp}, L_{box}, L_{rot}, L_{sem}, L_{mot}$ are the task-specific losses, and $w_i \in [0.98, 0.95, 0.90, 0.85, 0.80]$ are the loss weights.

B. Evaluation

Our experiments compare single-task learning (STL) against multi-task learning (MTL) for object detection, semantic segmentation, and motion segmentation on the KITTI dataset in Table I. For STL, each task is trained independently. With MTL, the tasks are trained jointly with shared parameters in the encoder backbone.

The MTL model shows significant gains over STL across all tasks. For object detection, MTL improves easy, moderate, and hard AP by **5.52%**, **6.22%**, and **4.76%**, respectively. For semantic segmentation, improvements of 1-3% IoU are obtained across all classes. Motion segmentation shows the most dramatic gains from MTL, with IoU increased by **20.5%** absolute from **52.6** to **73.1**. This highlights the synergies obtained when learning the tasks together. Since most moving objects are cars, the additional features learned by the other two tasks contribute to motion segmentation. Also, using an

TABLE I: **Quantitative comparison of Single-Task Learning (STL) and Multi-Task learning (MTL)** - Object detection (OD) (Average Precision (AP)), Semantic Segmentation (SS) (IoU), Motion segmentation (MS) (IoU) and Inference speed in Frames Per Second (FPS). Object detection and Motion segmentation show the largest gains from MTL.

Tasks			Object Detection			Semantic Segmentation				Motion
OD	SS	MS	Easy	Moderate	Hard	Car	Road	Building	Veg.	Seg.
✓	✗	✗	90.82	87.78	85.25	-	-	-	-	-
✗	✓	✗	-	-	-	94.01	96.76	80.04	81.00	-
✗	✗	✓	-	-	-	-	-	-	-	52.60
✓	✓	✓	95.40	93.00	87.13	95.10	95.78	82.10	83.33	-
✗	✓	✓	-	-	-	95.10	96.33	81.11	82.50	68.12
✓	✓	✓	96.34	94.00	90.01	96.18	96.12	84.50	81.09	73.14

additional past frame contributes directly to better performance.

While there are other multi-task learning approaches for autonomous driving perception, we could not find prior work tackling these three tasks on KITTI and SemanticKITTI in a joint framework. The improvements are attributable to shared representations in the encoder, improved regularization, and the inductive bias from training signals for related tasks. As shown in Table I, the multi-task approach outperforms single-task learning across object detection, semantic segmentation, and motion segmentation metrics. The only exception is road segmentation IoU, where STL has a slight 0.6% edge. A reasonable explanation for the consistent improvements from MTL is that the additional guidance from related semantic and motion features helps regularize the model and improve generalization. Our results validate multi-task learning as an effective paradigm for combined perception in autonomous driving.

We also compare our proposed LiDAR-BEVMTN against other LiDAR-only object detection methods on the KITTI benchmark. Table II shows results using average precision (AP) at an IoU threshold of 0.5, and Figure 5 shows the qualitative results. Figure 4 shows some of the failure cases of single-task networks, which are improved upon by the proposed multi-task approach. LiDAR-BEVMTN achieves **96.34AP** on the easy split, on par with top-performing SE-SSD at **97.7AP**. Our approach obtains state-of-the-art performance for the moderate category at **94.0AP**, a **0.7** point improvement over the prior best TED-S. While TED-S remains top for the hard category, LiDAR-BEVMTN attains a competitive **90.01AP**, just 2.1 points behind.

The strong performance of LiDAR-BEVMTN can be attributed to its multi-task learning framework. By training object detection jointly with semantic and motion segmentation in a shared model, the representation learns to encode spatial details, semantics, and motion cues. This provides a robust feature space for accurate 3D localization and orientation estimation. The results validate the benefits of multi-task inductive transfer for object detection from point cloud data.

Table III compares our LiDAR-BEVMTN to other LiDAR-based approaches on the SemanticKITTI validation set using intersection-over-union (IoU). LiDAR-BEVMTN achieves state-of-the-art performance for cars with **96.18%** IoU, out-

TABLE II: **Object detection’s IoU comparison** - Average Precision (AP) at IoU=0.5 against other single task approaches. We consider LiDAR only methods for comparison.

Models	Object Detection IoU = 0.5		
	Easy	Moderate	Hard
TED-S [49]	96.60	93.30	92.15
SE-SSD [22]	97.70	93.40	90.85
PART-A2 [50]	92.24	90.70	89.18
Point-RCNN [11]	90.20	89.63	89.39
LiDAR-BEVMTN	96.34	94.00	90.01

TABLE III: **Intersection over Union (IoU) comparison for semantic segmentation on SemanticKITTI validation set**

Models	Semantic Segmentation - IoU			
	Car	Road	Building	Veg.
Cylinder3D [51]	95.35	93.36	90.33	88.37
Point-Voxel-KD [32]	96.10	91.40	91.00	85.60
SalsaNext [52]	91.80	91.50	90.20	81.80
RangeNet++ [30]	91.40	91.80	87.40	80.50
LiDAR-BEVMTN	96.18	96.12	84.50	81.09

performing the next best Cylinder3D by **0.83%**. Our model also sets a new state-of-the-art for road segmentation at **96.12%** IoU. LiDAR-BEVMTN obtains competitive performance for vegetation, behind only Cylinder3D, by **0.28%**. On buildings, our approach attains **84.5%** IoU, lower than Point-Voxel-KD and Cylinder3D, which incorporate structural priors. The strong semantic segmentation capabilities of LiDAR-BEVMTN can be attributed to its multi-task learning framework. The model learns a spatially and contextually enriched representation by training jointly with related tasks like object detection. This provides a robust encoder space for accurate per-point semantic prediction. Our experiments validate multi-task learning as a practical paradigm for semantic segmentation from point cloud data.

Table IV compares our LiDAR-BEVMTN to other LiDAR-based moving object segmentation methods on the SemanticKITTI validation set. Using just **3** previous frames, LiDAR-BEVMTN achieves state-of-the-art performance with **73.14%** IoU, outperforming the next best RVMOS (**71.2%** with **5** frames) that utilizes more history. Compared to other approaches using **8 – 10** past frames, our model with **3** frames still shows substantial gains of **7 – 10%** IoU.

The strong motion segmentation capabilities of LiDAR-BEVMTN can be attributed to its multi-task learning framework, surpassing existing state-of-the-art methods. The model learns spatial and temporal features useful for tracking motion by training jointly with related perception tasks. This provides a robust encoder space for accurate per-point moving object prediction with minimal history. Our experiments validate the benefits of multi-task representation learning for motion segmentation from point cloud sequences.

Our ablation studies in Table V analyze the impact of the proposed SWAG module and point cloud densification on object detection, semantic segmentation, and motion segmentation. Using SWAG improves object detection AP in easy, moderate, and hard categories by **0.5 – 1.4%** absolute. This supports our hypothesis that incorporating weighted semantic

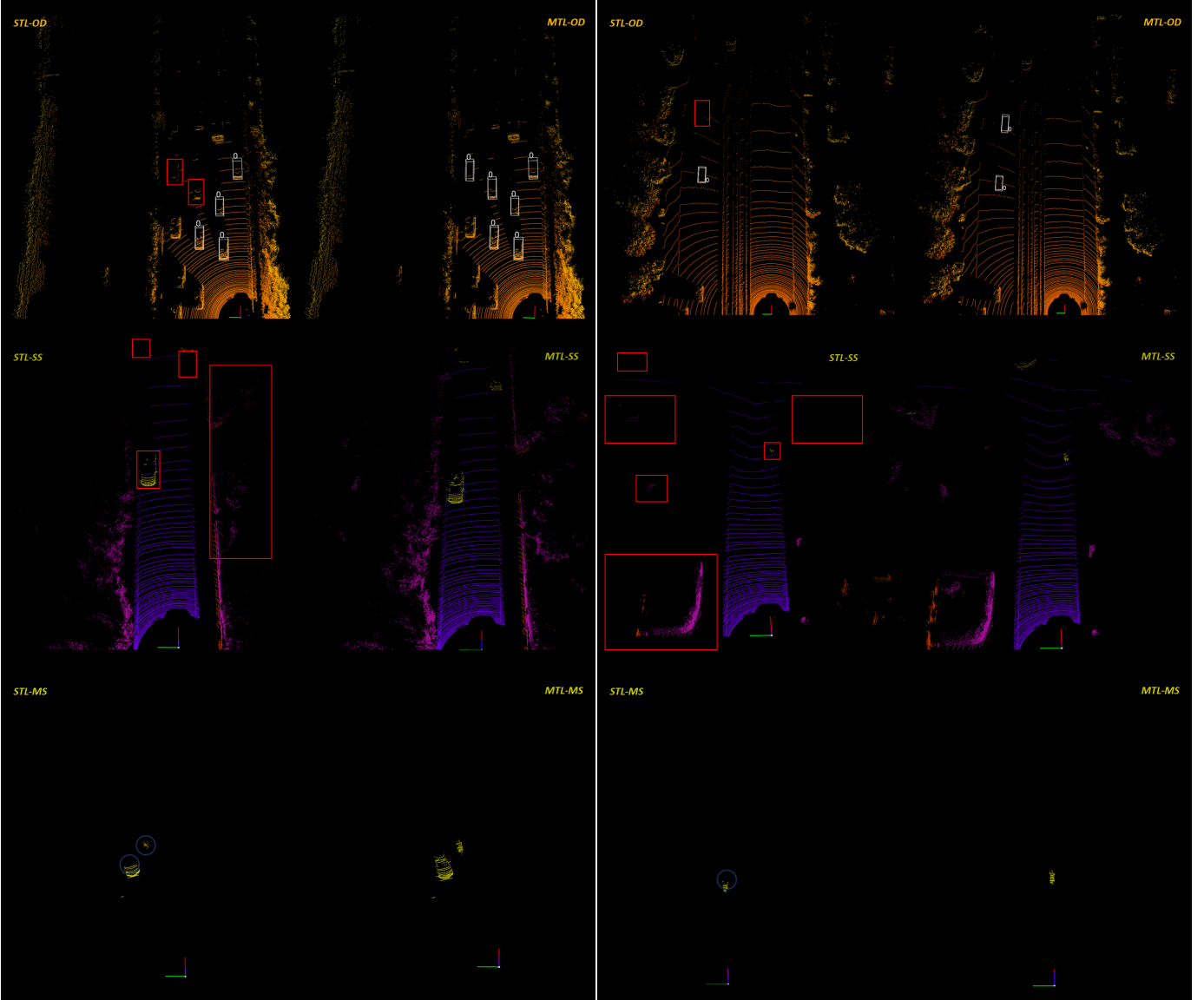


Fig. 4: **Qualitative results for performance comparison** - Multi Task Lidar (MTL) and Single Task LiDAR (STL) approaches for Object Detection (OD), Semantic Segmentation(SS), and Motion Segmentation (MS). The MTL approach improves all tasks for the shown failure cases of STL. The results can be further viewed in high-quality; see <https://youtu.be/H-hWRzv2IIY>

TABLE IV: **Intersection over Union (IoU) comparison for moving object segmentation on the SemanticKITTI validation set (seq 08)**. The number of past frames used by each method is shown under history.

Models	Motion Segmentation	
	History	IoU
RVMOS [53]	5	71.20
MotionSeg3D [35]	8	65.20
4DMOS [54]	10	65.20
LMNet [33]	8	62.50
LiMoSeg [34]	2	52.60
LiDAR-BEVMTN	3	73.14

features benefits object detection. SWAG also provides small IoU gains of 0.5 – 1.3% for semantic segmentation across cars, roads, and buildings. SWAG consistently improves the utilization of semantic features, benefiting object detection

TABLE V: **Ablation: Effect of semantic guidance and range-based point cloud densification on different tasks**. Point cloud augmentation was not applied to segmentation tasks.

Param.	Object Detection			Semantic Segmentation				Motion Seg.	
	SWAG	Densif.		Easy	Moderate	Hard	Car		Road
×	×	93.01	90.49	87.04	94.14	94.26	83.22	81.49	71.12
×	✓	94.81	92.19	88.10	NA	NA	NA	NA	NA
✓	×	93.50	91.34	88.12	96.15	96.12	84.50	81.10	73.01
✓	✓	96.34	94.00	90.01	96.18	96.12	84.50	81.09	73.14

and semantic segmentation. Point cloud densification shows marginal AP improvements of 0.8 – 1.9% in moderate and hard object detection categories, at the cost of a 1.2% drop in easy. This mixed impact is likely because densification was only applied to object detection inputs during multi-task training. The variation in BEV input causes negative effects

TABLE VI: **Inference latency comparison-** Multi Task LiDAR (MTL) and Single Task LiDAR (STL) networks for Object Detection (OD), Semantic Segmentation (SS), and Motion Segmentation (MS). MTL - 3 tasks achieves 3x speed up over three single task networks.

Task combination	FP16 Inference Latency (ms)	Speedup factor
STL(OD) + STL(SS) + STL(MS)	8.80	baseline
STL(OD) + MTL(SS + MS)	5.65	1.55
STL(MS) + MTL(OD + SS)	5.83	1.50
MTL(OD + SS + MS)	3.01	2.92

on joint learning. Point cloud densification shows potential but needs a unified augmentation strategy across tasks.

Table VI compares the inference latency of our multi-task LiDAR-BEVMN against single-task LiDAR networks for object detection, semantic segmentation, and motion segmentation. Using three separate single-task models for the three tasks takes **8.80ms** per frame. Combining two tasks under multi-task learning reduces latency to **5.65 – 5.83ms**, a **1.5 – 1.55x** speedup. Finally, with our full multi-task model concurrently performing object detection, semantic segmentation, and motion segmentation, inference time is reduced to just **3.01ms** per frame - a **2.92x** speedup over separate single-task networks.

The substantial latency improvements of LiDAR-BEVMN can be attributed to computation sharing in the unified encoder-decoder network. Features are extracted just once from the LiDAR point cloud and reused across all heads. This avoids expensive redundant feature extraction for each task. Our experiments validate multi-task learning as an effective approach to improve computational efficiency and enable real-time performance for combined 3D perception from point cloud data.

V. CONCLUSION

In this work, we have presented LiDARBEVMN, a multi-task neural network for joint object detection, semantic segmentation, and motion segmentation from LiDAR point clouds. Our proposed model achieves state-of-the-art results across all three tasks on the challenging KITTI and SemanticKITTI datasets. To the best of our knowledge, this is the first work to tackle these specific tasks together using multi-task deep learning on KITTI and SemanticKITTI. Our results and analyses demonstrate the advantages of multi-task learning for combined 3D perception. Despite multiple tasks using consecutive LiDAR scans, we achieved a low latency of 3 ms on an embedded automotive platform. Future work includes extending this approach to other perception tasks like odometry, ego-motion estimation, and velocity prediction for autonomous driving. We hope this work provides useful insights and motivates continued research into multi-task deep learning for LiDAR-based scene understanding.

REFERENCES

[1] L. Joseph and A. K. Mondal, *Autonomous driving and Advanced Driver-Assistance Systems (ADAS): applications, development, legal issues, and testing*. CRC Press, 2021.

[2] V. R. Kumar, S. Milz, C. Witt, M. Simon *et al.*, “Near-field depth estimation using monocular fisheye camera: A semi-supervised learning approach using sparse LiDAR data,” in *CVPR Workshop*, vol. 7, 2018, p. 2.

[3] V. R. Kumar, M. Klingner, S. Yogamani, M. Bach *et al.*, “SVDistNet: Self-supervised near-field distance estimation on surround view fisheye cameras,” *IEEE Transactions on Intelligent Transportation Systems*, vol. 23, no. 8, pp. 10252–10261, 2021.

[4] M. Uricár, D. Hurych, P. Krizek, and S. Yogamani, “Challenges in designing datasets and validation for autonomous driving,” *arXiv preprint arXiv:1901.09270*, 2019.

[5] M. Uricár, J. Ulicny, G. Sistu, H. Rashed *et al.*, “Desoiling dataset: Restoring soiled areas on automotive fisheye cameras,” in *Proceedings of the IEEE/CVF International Conference on Computer Vision Workshops*, 2019, pp. 0–0.

[6] M. M. Dhananjaya, V. R. Kumar, and S. Yogamani, “Weather and light level classification for autonomous driving: Dataset, baseline and active learning,” in *2021 IEEE International Intelligent Transportation Systems Conference (ITSC)*. IEEE, 2021, pp. 2816–2821.

[7] Y. Zhou and O. Tuzel, “Voxelnet: End-to-end learning for point cloud based 3d object detection,” in *Proceedings of the IEEE conference on computer vision and pattern recognition*, 2018, pp. 4490–4499.

[8] D. Maturana and S. Scherer, “Voxnet: A 3d convolutional neural network for real-time object recognition,” in *2015 IEEE/RSJ international conference on intelligent robots and systems (IROS)*. IEEE, 2015, pp. 922–928.

[9] Y. Yan, Y. Mao, and B. Li, “Second: Sparsely embedded convolutional detection,” *Sensors*, vol. 18, no. 10, p. 3337, 2018.

[10] A. Geiger, P. Lenz, C. Stiller, and R. Urtasun, “Vision meets robotics: The kitti dataset,” *The International Journal of Robotics Research*, vol. 32, no. 11, pp. 1231–1237, 2013.

[11] S. Shi, X. Wang, and H. Li, “Pointtrnn: 3d object proposal generation and detection from point cloud,” in *Proceedings of the IEEE/CVF conference on computer vision and pattern recognition*, 2019, pp. 770–779.

[12] C. R. Qi, L. Yi, H. Su, and L. J. Guibas, “Pointnet++: Deep hierarchical feature learning on point sets in a metric space,” *Advances in neural information processing systems*, vol. 30, 2017.

[13] S. Shi, C. Guo, L. Jiang, Z. Wang *et al.*, “Pv-rcnn: Point-voxel feature set abstraction for 3d object detection,” in *Proceedings of the IEEE/CVF Conference on Computer Vision and Pattern Recognition*, 2020, pp. 10 529–10 538.

[14] P. Sun, H. Kretzschmar, X. Dotiwala, A. Chouard *et al.*, “Scalability in perception for autonomous driving: Waymo open dataset,” in *Proceedings of the IEEE/CVF conference on computer vision and pattern recognition*, 2020, pp. 2446–2454.

[15] X. Wu, L. Peng, H. Yang, L. Xie *et al.*, “Sparse fuse dense: Towards high quality 3d detection with depth completion,” in *Proceedings of the IEEE/CVF Conference on Computer Vision and Pattern Recognition*, 2022, pp. 5418–5427.

[16] S. Borse, M. Klingner, V. R. Kumar, H. Cai *et al.*, “X-Align: Cross-Modal Cross-View Alignment for Bird’s-Eye-View Segmentation,” in *Proceedings of the IEEE/CVF Winter Conference on Applications of Computer Vision*, 2023, pp. 3287–3297.

[17] S. Mohapatra, S. Yogamani, H. Gotzig, S. Milz *et al.*, “BEVDetNet: bird’s eye view LiDAR point cloud based real-time 3D object detection for autonomous driving,” in *2021 IEEE International Intelligent Transportation Systems Conference (ITSC)*. IEEE, 2021, pp. 2809–2815.

[18] B. Yang, W. Luo, and R. Urtasun, “Pixor: Real-time 3d object detection from point clouds,” in *Proceedings of the IEEE conference on Computer Vision and Pattern Recognition*, 2018, pp. 7652–7660.

[19] M. Simony, S. Milzy, K. Amendey, and H.-M. Gross, “Complex-yolo: An euler-region-proposal for real-time 3d object detection on point clouds,” in *Proceedings of the European Conference on Computer Vision (ECCV) Workshops*, 2018, pp. 0–0.

[20] A. H. Lang, S. Vora, H. Caesar, L. Zhou *et al.*, “Pointpillars: Fast encoders for object detection from point clouds,” in *Proceedings of the IEEE/CVF conference on computer vision and pattern recognition*, 2019, pp. 12 697–12 705.

[21] W. Liu, D. Anguelov, D. Erhan, C. Szegedy *et al.*, “Ssd: Single shot multibox detector,” in *European conference on computer vision*. Springer, 2016, pp. 21–37.

[22] W. Zheng, W. Tang, L. Jiang, and C.-W. Fu, “SE-SSD: Self-ensembling single-stage object detector from point cloud,” in *Proceedings of the IEEE/CVF Conference on Computer Vision and Pattern Recognition*, 2021, pp. 14 494–14 503.

- [23] P. Dutta, G. Sistu, S. Yogamani, E. Galván *et al.*, “ViT-BEVSeg: A hierarchical transformer network for monocular birds-eye-view segmentation,” in *2022 International Joint Conference on Neural Networks (IJCNN)*. IEEE, 2022, pp. 1–7.
- [24] H. Rashed, A. El Sallab, S. Yogamani, and M. ElHelw, “Motion and depth augmented semantic segmentation for autonomous navigation,” in *Proceedings of the IEEE/CVF Conference on Computer Vision and Pattern Recognition Workshops*, 2019, pp. 0–0.
- [25] J. Behley, M. Garbade, A. Milioto, J. Quenzel *et al.*, “Semantickitti: A dataset for semantic scene understanding of lidar sequences,” in *Proceedings of the IEEE/CVF International Conference on Computer Vision*, 2019, pp. 9297–9307.
- [26] B. Wu, A. Wan, X. Yue, and K. Keutzer, “Squeezeseg: Convolutional neural nets with recurrent crf for real-time road-object segmentation from 3d lidar point cloud,” in *2018 IEEE International Conference on Robotics and Automation (ICRA)*. IEEE, 2018, pp. 1887–1893.
- [27] B. Wu, X. Zhou, S. Zhao, X. Yue *et al.*, “Squeezesegv2: Improved model structure and unsupervised domain adaptation for road-object segmentation from a lidar point cloud,” in *2019 International Conference on Robotics and Automation (ICRA)*. IEEE, 2019, pp. 4376–4382.
- [28] F. N. Iandola, S. Han, M. W. Moskewicz, K. Ashraf *et al.*, “SqueezeNet: AlexNet-level accuracy with 50x fewer parameters and 0.5 MB model size,” *arXiv preprint arXiv:1602.07360*, 2016.
- [29] S. Zheng, S. Jayasumana, B. Romera-Paredes, V. Vineet *et al.*, “Conditional random fields as recurrent neural networks,” in *Proceedings of the IEEE international conference on computer vision*, 2015, pp. 1529–1537.
- [30] A. Milioto, I. Vizzo, J. Behley, and C. Stachniss, “Rangenet++: Fast and accurate lidar semantic segmentation,” in *2019 IEEE/RSJ international conference on intelligent robots and systems (IROS)*. IEEE, 2019, pp. 4213–4220.
- [31] J. Redmon and A. Farhadi, “Yolov3: An incremental improvement,” *arXiv preprint arXiv:1804.02767*, 2018.
- [32] Y. Hou, X. Zhu, Y. Ma, C. C. Loy *et al.*, “Point-to-voxel knowledge distillation for lidar semantic segmentation,” in *Proceedings of the IEEE/CVF Conference on Computer Vision and Pattern Recognition*, 2022, pp. 8479–8488.
- [33] X. Chen, S. Li, B. Mersch, L. Wiesmann *et al.*, “Moving object segmentation in 3D LiDAR data: A learning-based approach exploiting sequential data,” *IEEE Robotics and Automation Letters*, vol. 6, no. 4, pp. 6529–6536, 2021.
- [34] S. Mohapatra, M. Hodaie, S. Yogamani, S. Milz *et al.*, “LiMoSeg: Real-time Bird’s Eye View based LiDAR Motion Segmentation,” *arXiv preprint arXiv:2111.04875*, 2021.
- [35] J. Sun, Y. Dai, X. Zhang, J. Xu *et al.*, “Efficient Spatial-Temporal Information Fusion for LiDAR-Based 3D Moving Object Segmentation,” in *2022 IEEE/RSJ International Conference on Intelligent Robots and Systems (IROS)*. IEEE, 2022, pp. 11 456–11 463.
- [36] I. Leang, G. Sistu, F. Bürger, A. Bursuc *et al.*, “Dynamic task weighting methods for multi-task networks in autonomous driving systems,” in *2020 IEEE 23rd International Conference on Intelligent Transportation Systems (ITSC)*. IEEE, 2020, pp. 1–8.
- [37] M. Klingner, V. R. Kumar, S. Yogamani, A. Bär *et al.*, “Detecting adversarial perturbations in multi-task perception,” in *2022 IEEE/RSJ International Conference on Intelligent Robots and Systems (IROS)*. IEEE, 2022, pp. 13 050–13 057.
- [38] Z. Liu, H. Tang, A. Amini, X. Yang *et al.*, “BEVFusion: Multi-Task Multi-Sensor Fusion with Unified Bird’s-Eye View Representation,” *arXiv preprint arXiv:2205.13542*, 2022.
- [39] D. Ye, Z. Zhou, W. Chen, Y. Xie *et al.*, “Lidarmultinet: Towards a unified multi-task network for lidar perception,” *arXiv preprint arXiv:2209.09385*, 2022.
- [40] F. Duffhauß and S. A. Baur, “PillarFlowNet: A real-time deep multitask network for LiDAR-based 3D object detection and scene flow estimation,” in *2020 IEEE/RSJ International Conference on Intelligent Robots and Systems (IROS)*. IEEE, 2020, pp. 10 734–10 741.
- [41] D. Feng, Y. Zhou, C. Xu, M. Tomizuka *et al.*, “A simple and efficient multi-task network for 3d object detection and road understanding,” in *2021 IEEE/RSJ International Conference on Intelligent Robots and Systems (IROS)*. IEEE, 2021, pp. 7067–7074.
- [42] V. R. Kumar, S. Yogamani, H. Rashed, G. Sistu *et al.*, “Omnidet: Surround view cameras based multi-task visual perception network for autonomous driving,” *IEEE Robotics and Automation Letters*, vol. 6, no. 2, pp. 2830–2837, 2021.
- [43] Z. Liu, H. Mao, C.-Y. Wu, C. Feichtenhofer *et al.*, “A convnet for the 2020s,” in *Proceedings of the IEEE/CVF conference on computer vision and pattern recognition*, 2022, pp. 11 976–11 986.
- [44] A. Paszke, S. Gross, S. Chintala, G. Chanan *et al.*, “Automatic differentiation in pytorch,” 2017.
- [45] D. P. Kingma and J. Ba, “Adam: A method for stochastic optimization,” *arXiv preprint arXiv:1412.6980*, 2014.
- [46] I. Loshchilov and F. Hutter, “Sgdr: Stochastic gradient descent with warm restarts,” *arXiv preprint arXiv:1608.03983*, 2016.
- [47] T.-Y. Lin, P. Goyal, R. Girshick, K. He *et al.*, “Focal loss for dense object detection,” in *Proceedings of the IEEE international conference on computer vision*, 2017, pp. 2980–2988.
- [48] R. Girshick, “Fast r-cnn,” in *Proceedings of the IEEE international conference on computer vision*, 2015, pp. 1440–1448.
- [49] H. Wu, C. Wen, W. Li, X. Li *et al.*, “Transformation-Equivariant 3D Object Detection for Autonomous Driving,” *arXiv preprint arXiv:2211.11962*, 2022.
- [50] S. Shi, Z. Wang, X. Wang, and H. Li, “Part-a² net: 3d part-aware and aggregation neural network for object detection from point cloud,” *arXiv preprint arXiv:1907.03670*, vol. 2, no. 3, 2019.
- [51] H. Zhou, X. Zhu, X. Song, Y. Ma *et al.*, “Cylinder3d: An effective 3d framework for driving-scene lidar semantic segmentation,” *arXiv preprint arXiv:2008.01550*, 2020.
- [52] T. Cortinhal, G. Tzelepis, and E. Erdal Aksoy, “Salsanext: Fast, uncertainty-aware semantic segmentation of lidar point clouds,” in *Advances in Visual Computing: 15th International Symposium, ISVC 2020, San Diego, CA, USA, October 5–7, 2020, Proceedings, Part II 15*. Springer, 2020, pp. 207–222.
- [53] J. Kim, J. Woo, and S. Im, “RVMOS: Range-View Moving Object Segmentation Leveraged by Semantic and Motion Features,” *IEEE Robotics and Automation Letters*, vol. 7, no. 3, pp. 8044–8051, 2022.
- [54] B. Mersch, X. Chen, I. Vizzo, L. Nunes *et al.*, “Receding moving object segmentation in 3d lidar data using sparse 4d convolutions,” *IEEE Robotics and Automation Letters*, vol. 7, no. 3, pp. 7503–7510, 2022.

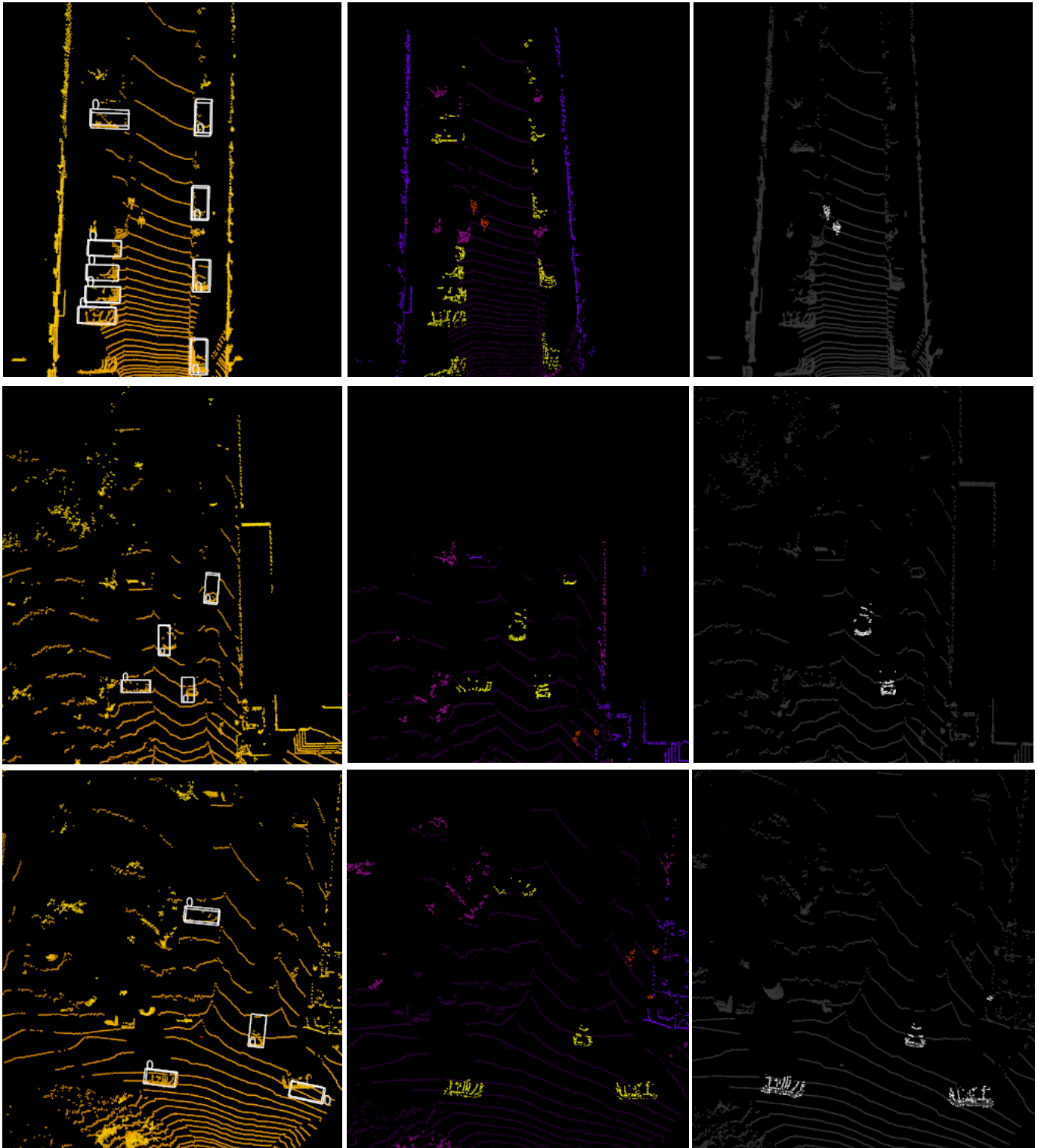


Fig. 5: Qualitative results for 3D object detection (left), semantic segmentation (middle), and motion segmentation (right) in SemanticKITTI dataset. Color coding scheme for segmentation - yellow for cars, purple for buildings, pink for vegetation, and motion segmentation - white denotes moving points.